Journal of Hydrology (2008) 362, 57–68

available at www.sciencedirect.com

ScienceDirect

journal homepage: www.elsevier.com/locate/jhydrol

# Estimation of laboratory-scale dispersivities using an annulus-and-core device

Christophe C. Frippiat [a,c,*], Patrick Conde Pérez [b], Alain E. Holeyman [c]

[a] *Center for Experimental Study of Subsurface Environmental Processes (CESEP), Colorado School of Mines, 1500 Illinois Street, Golden, CO 80401, USA*
[b] *SECO S.C., Brussels, Belgium*
[c] *Department of Civil and Environmental Engineering, Université catholique de Louvain, Louvain-la-Neuve, Belgium*

Received 16 March 2008; received in revised form 4 August 2008; accepted 13 August 2008

**KEYWORDS**
Laboratory methods;
Annulus-and-core tests;
Longitudinal dispersivity;
Transverse dispersivity

**Summary** This paper investigates the use of two-dimensional radial column experiments to estimate longitudinal and transverse dispersivity at the laboratory scale. The experimental device is an ''annulus-and-core'' device: it is based on a classical column system, of which the inlet reservoir is divided into three independent concentric zones, allowing non-uniform tracer injection. The outlet reservoir is similarly adapted, so that information on the radial distribution of concentration becomes available through mean effluent concentration measurements in each annular zone. In this study, we only investigated continuous tracer injections through the central inlet zone. An analytical solution to a similar problem was available in the literature, and was adapted to compute effluent concentrations. The influence of the simplified boundary conditions of the solution was assessed by means of a numerical model. A general methodology is suggested to obtain transport parameters from breakthrough curve analysis, involving (i) the determination of effective porosity and longitudinal dispersivity from the full averaged breakthrough curve using classical one-dimensional tools and (ii) the determination of transverse dispersivity from the breakthrough curves recorded in the annular zones. Preliminary experiments were performed on a glass bead porous medium, on a gravel sand and on a natural medium sand. It is found that the rapidity of the test, its low cost, and the ability to simultaneously estimate three transport parameters comes at the price of potentially larger experimental errors. Transverse dispersivities were found to be higher than values previously reported in the literature, probably as a result of plume meandering, which cannot be detected nor corrected when using annulus-and-core devices.


* Corresponding author. Address: Center for Experimental Study of Subsurface Environmental Processes (CESEP), Colorado School of Mines, 1500 Illinois Street, Golden, CO 80401, USA. Tel.: +1 303 384 2237.
*E-mail address:* cfrippia@mines.edu (C.C. Frippiat).

0022-1694/$ - see front matter © 2008 Elsevier B.V. All rights reserved.
doi:10.1016/j.jhydrol.2008.08.007

## Introduction

Longitudinal dispersivity has been a major research topic in subsurface hydrology for a few decades and a great amount of data is currently available in the literature (see e.g. the recent compilations by Schulze-Makuch (2005) and by Bromly et al. (2007)). By contrast, few measures of transverse dispersivity have been made, even though it has crucial importance when modeling transport in physically heterogeneous media (Gelhar et al., 1979), multispecies transport (Cirpka et al., 2006), multiphase transport (Oostrom et al., 1992, 1999a,b; Seagren et al., 1999) or microbial activity in aquifers (Cirpka et al., 1999).

Existing methods to estimate transverse dispersion are usually based either on tracer tests (either at the laboratory or at the field scale) or on dissolution tests (at the laboratory scale). Dissolution tests generally imply groundwater flow along a stagnant zone containing constant concentration gas (Klenk and Grathwohl, 2002; McCarthy and Johnson, 1993), NAPL (Oostrom et al., 1999a,b; Pearce et al., 1994) or solid (Guedes de Carvalho and Delgado, 1999, 2000; Delgado and Guedes de Carvalho, 2001). Transverse dispersivity can then be inferred from the rate of dissolution of the third phase, which is obtained through solute breakthrough curve measurements at the laboratory model outlet.

Most of the tracer tests designed to determine transverse dispersion coefficients are performed in a uniform flow at constant mean velocity. Blackwell (1962) and Hassinger and von Rosenberg (1968) used the so-called ''annulus-and-core'' approach, in which the inlet and the outlet cross-sections of a column are divided into two concentric zones. The concentration of the solution flowing in the inner inlet zone (the core) is rapidly increased, while the solution in the outer inlet zone (the annulus) is kept solute-free. Transverse dispersivity is computed by comparing the steady-state concentration of effluent solutions in the outlet annulus and core zones. Divided inlets were also adopted in several other column studies involving intrusive local concentration measurements (Bruch, 1970; Grane and Gardner, 1961; Han et al., 1985; Harleman and Rumer, 1963; Perkins and Johnston, 1963; Zhang et al., 2006). Grid lysimeter devices, used to study water flow and solute transport in the vadose zone, have a divided outlet. A sampling grid is installed at the bottom of the lysimeter, allowing local surface-averaged measurements of water fluxes and solute concentrations (e.g. de Rooij and Stagnitti, 2002). Other authors preferred point injection, either in column (Olsson and Grathwohl, 2007; Pisani and Tosi, 1994; Robbins, 1989) or in the field (Jiao, 1993; Kelly et al., 1994; Zou and Parr, 1993, 1994). A few specific devices imply non-uniform flow: Cirpka and Kitanidis (2001) and Benekos et al. (2006) investigated flow and transport in a helix and in a cochlea to determine transverse dispersivity. Kim et al. (2004) determined local longitudinal and transverse dispersivities in a laboratory aquifer model with a local recharge zone.

In this paper, we use an ''annulus-and-core'' method similar to that of Blackwell (1962) and Hassinger and von Rosenberg (1968). We have modified the device by dividing inlet and outlet flasks into three concentric zones rather than two (Fig. 1). Recently, Massabo et al. (2006) have proposed a set of analytical solutions for two-dimensional advection–dispersion problems in axisymmetrical geometries of finite lateral extent. These solutions include among others concentration distributions resulting from the continuous injection of tracer in a circular zone centered on the longitudinal axis of the column. That particular solution was adapted to interpret effluent concentration data recorded in the three outlet zones. It must be noted that Massabo et al. (2006) have developed these solutions within the framework of similar experiments, based however on non-intrusive electrical measurements along the column body. As an example of application, three porous materials are tested: glass beads, a gravel sand and a natural medium sand.

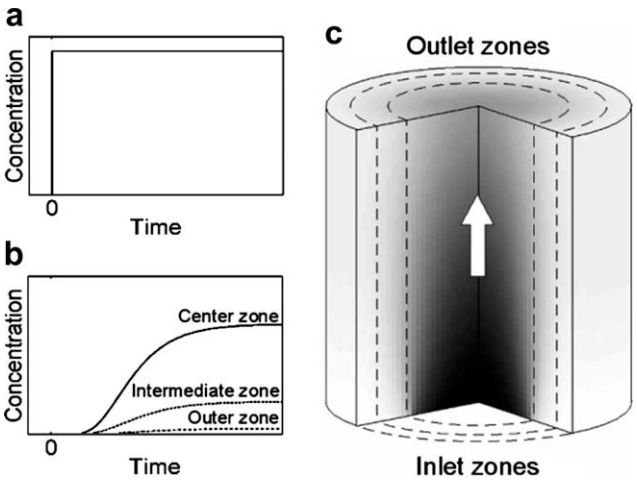


**Figure 1** Concentration distributions within an annulus-and-core device with three inlet and outlet zones. (a) Continuous injection through the central inlet zone. (b) Resulting breakthrough curves in the three outlet zones. (c) Three-dimensional spatial distribution of concentration within the column at an intermediate time.

## Experimental setup and materials

The experimental setup is based on a classical column system used to determine longitudinal transport properties. The setup is illustrated in Fig. 2. The column consists of a Plexiglas pipe of length $L = 11.63$ cm and of inner diameter $D = 10.14$ cm (radius $R = 5.07$ cm). The inlet reservoir is divided into three independent concentric zones in order to perform two-dimensional tests. Each zone has an equal cross-sectional surface area and is supplied with two specific tubes allowing solution feeding and pressure measurement. The central circular zone has a radius $R_1 = 2.93$ cm and the intermediate annular zone has an outer radius $R_2 = 4.14$ cm. The pipe is covered with a thin layer of silicon grease to minimize wall effects resulting from the higher porosity close to the lateral boundaries. The inlet boundary is made of stainless steel (quality AISI 316L) screened with 80 holes of 3-mm-diameter evenly distributed along the surface of each zone. Additional filters are also used to prevent finest grains from flowing out of the column. The mesh size of the filters is adapted to the particle size distribution of the material tested. The outlet reservoir is similarly modified, so that the concentration responses of the system partitions can be individually recorded. It must be noted that

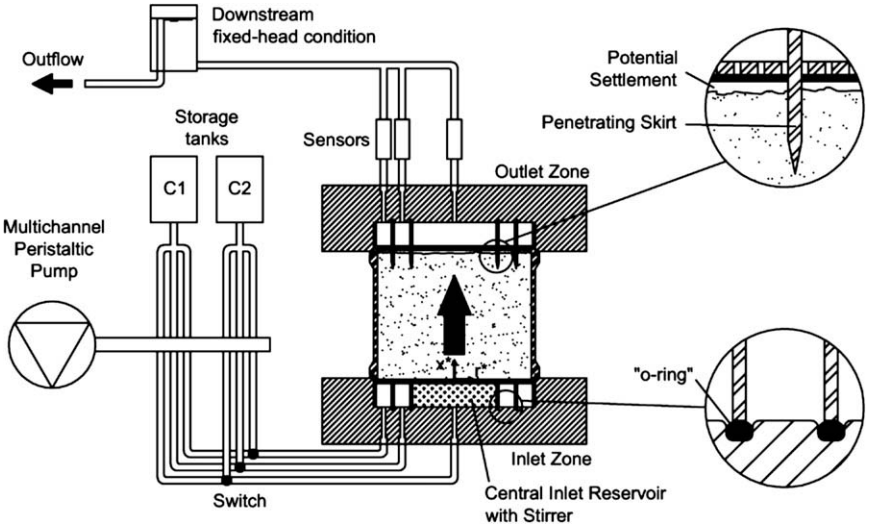


**Figure 2** Sketch of the experimental setup.

the outlet reservoir is equipped with 15 mm long skirts penetrating the sample (see the detail in Fig. 2) in order to prevent hydraulic short-circuiting resulting from potential sample settlement in the column. Practically, the feeding valves are directly placed on the Plexiglas reservoir, so that tube lengths to inlet zones are minimized. Moreover, the injection zone is equipped with a magnetic stirrer in order to ensure proper mixing in the upstream reservoir (Novakowski, 1992a,b; van Genuchten and Parker, 1984).

Concentration and hydraulic head can be imposed individually in each zone of the column, leading to a large number of possible two-dimensional injection schemes. However, only uniform flow with continuous injection of tracer in the central inlet reservoir is investigated in this study. A 6-roller multichannel peristaltic pump (Ismatec MCP V5.16 with 3.17 mm diameter Tygon tubing) is used to feed each upstream zone at an equal rate. It is expected that the use of 6 rollers (instead of 3, for example, on standard pumps) minimizes pulse effects, believed to cause additional dispersion. Since the flow rate of a peristaltic pump is affected by the state of the tubing, they were rotated on a regular time basis to maintain all of them in a similar state and ensure similar flow rates in each zone. New tubing was also installed on a regular time basis. The three downstream zones are connected to a single constant-head reservoir. Effluent concentrations are monitored in each outlet zone using custom inline conductivity probes. The effluent solution passes through a stainless steel tube (quality AISI 316L) being the first electrode of the sensor. The second one is a perpendicular stainless steel needle that is electrically isolated from the first electrode. Sensors are supplied with a sinusoidal current $I = 1$ mA at a frequency of 1 kHz, in order to avoid electrode polarization effects. The probes are calibrated with NaCl solutions within the range of observed concentrations (from 0.5 to 1 g/l) and within a temperature range corresponding to normal use (from 20 to 25 °C). In a first step, quadratic regressions are used to link the inverse of measured electric potential to solution electrical conductivity $\sigma$. Then, electrical conductivity is converted into NaCl concentration $C$ using a temperature-dependent law $\sigma = aT + bC + cCT + d$, where $T$ is the temperature and $a$, $b$, $c$ and $d$ are calibrated constants.

The setup is tested using three different porous materials: glass beads, a gravel sand and a medium sand (Table 1). Glass beads are used to keep a point of comparison with the numerous studies on transverse dispersion reported in the literature (Baumeister et al., 1995; Delgado and Guedes de Carvalho, 2001; Guedes de Carvalho and Delgado, 1999, 2000; Grane and Gardner, 1961; Han et al., 1985; Harleman and Rumer, 1963; Olsson and Grathwohl, 2007; Robbins, 1989; Xu and Eckstein, 1997). We use a mix of 50% of SB 30 and 50% SB 40 glass beads from Sovitec France, resulting in a material with a particle size linearly distributed between 1 mm and 2 mm. The gravel sand we tested (Quartz 1/2 from J. Tielen Minerals, Belgium) has a mean grain

**Table 1** Physical and hydraulic properties of tested materials

| Property | Glass beads | Gravel sand | Brusselean sand |
|---|---|---|---|
| Specific weight, $\gamma_s$ (kN/m$^3$) | 25.31 | 25.75 | 25.98 |
| Mean grain diameter, $d_{50}$ (μm) | 1445 | 1540 | 315 |
| Uniformity coefficient, $Cu = d_{60}/d_{10}$ (−) | 1.42 | 1.69 | 2.43 |
| Total porosity, $n$ (%) | 34.2—40.6 | 39.2—40.2 | 36.0—37.1 |
| Hydraulic conductivity[a], $K$ (mm/s) | 12.8 | 15.4 | 0.23—0.36 |

[a] Determined using a column device and a packing method similar to those used in this study.

diameter similar to that of the glass beads, but has a broader particle size distribution. Since its porosity is usually larger than that of the glass beads, its hydraulic conductivity is also slightly larger. Finally, we use Brusselean sand, a natural sand outcropping in the area of Brussels (Belgium) and largely present in the entire Walloon Brabant province. The Brusselean sand used in this study was collected in a quarry located about 30 km south of Brussels. Its mean grain size is half an order of magnitude smaller than that of the other tested materials and its grain size distribution is the broadest, as indicated by its larger uniformity coefficient.

Sand samples are compacted at low water content (between 5% and 10%) in three layers, using a sliding weight hammer. This method is based on the modified Proctor procedure (ASTM D1557, 2002). Although thinner layers are generally recommended for the production of homogeneous samples (Oliviera et al., 1996), the use of a heavy 2.5 kg steel weight allowed a dense packing, with relatively smaller density variations. Since using this methodology with glass beads could yield particle crushing, the beads are only dry vibrated. The samples are saturated using a procedure similar to the recommended method for the preparation of samples for the determination of hydraulic conductivity of granular soils (ASTM D2434-68, 2000). First, a negative pressure of about 50 cm of Hg is applied on the sample using a vacuum pump during 15 min. Demineralized water is then introduced in the sample from the bottom, at a low rate. The water was not deaired, and no replacement by $CO_2$ of air within the column prior to saturation was performed. However, saturation was checked by weighing the full device prior and after the procedure, knowing the dry mass of the soil sample, its initial saturation, and the weight of the column device. The procedure is repeated until a saturation larger than 95% is obtained.

Once saturation is reached, steady-state flow with a solution at a concentration of about 0.5 g/l NaCl is established. A zero-conductivity measurement would correspond to an infinite voltage, which cannot be measured. We chose a background concentration leading to an electrical conductivity similar to that of tap water. For each sample, two or three steps in concentration are performed, with concentration increments between 0.1 g/l and 0.2 g/l. This results from a compromise between additional noise on measurements, resulting e.g. from ambient temperature variations, and density effects, known to occur at concentration as low as 0.05 g/l (Istok and Humphrey, 1995).

## Analysis of effluent concentration data

In this section, we develop a methodology to analyze concentration data obtained using the experimental setup described previously. First, an analytical solution for effluent concentrations in outlet zones is derived based on the developments of Massabo et al. (2006). Then, the effect of simplified boundary conditions used to derive the analytical solution is investigated using a numerical model, and the resulting bias on estimated transport parameters is shown to be insignificant compared to other potential experimental errors. Finally, a general methodology is suggested to analyze experimental data accounting for the effect of flask volumes and actual injection conditions.

### Analytical solution

The advection–dispersion equation expressed in a cylindrical coordinate system reads

$$\frac{\partial C^*}{\partial t^*} = -v\frac{\partial C^*}{\partial x^*} + D_L\frac{\partial^2 C^*}{\partial x^{*2}} + D_T\left(\frac{\partial^2 C^*}{\partial r^{*2}} + \frac{1}{r^*}\frac{\partial C^*}{\partial r^*}\right) \tag{1}$$

where $C^*$ is the concentration, $v$ is the longitudinal velocity, $D_L$ and $D_T$ are longitudinal and transverse dispersion coefficients respectively. $t^*$ is the time and $x^*$ and $r^*$ are longitudinal and radial positions, respectively. A continuous injection through the inlet central zone at a concentration $C_0$ is modeled using a first-type boundary condition (i.e. a constant concentration boundary condition)

$$C^*(0, r^*, t^*) = C_{init} + H(t^*) \times \begin{cases} C_0 - C_{init} & \text{if } 0 \leqslant r^* < R_1 \\ \frac{C_0 - C_{init}}{2} & \text{if } r^* = R_1 \\ 0 & \text{if } R_1 < r^* \leqslant R \end{cases} \tag{2a}$$

where $R_1$ is the radius of the central inlet zone and $H(t^*)$ is the Heaviside (step) function. $C_{init}$ is the uniform initial concentration. van Genuchten and Parker (1984) showed that an injection condition such as (2a) does not verify mass balance across the inlet boundary of the column. However, for one-dimensional problems, a first-type boundary condition can be adopted provided tracer injection and detection both occur in flux (Kreft and Zuber, 1978; van Genuchten and Parker, 1984). The appropriateness of (2a) will be further investigated with the aid of the numerical model developed below. Additional boundary conditions are

$$\left.\frac{\partial C^*(x^*, r^*, t^*)}{\partial r^*}\right|_{r^*=R} = 0 \tag{2b}$$

$$\lim_{x^*\to\infty} C(x^*, r^*, t^*) = 0 \tag{2c}$$

with $R$ being the radius of the column. The boundary condition in Eq. (2c) therefore states that the column is assumed to be of infinite length. The problem defined by Eq. (1) can be written using dimensionless variables

$$\frac{\partial C}{\partial t} = -\frac{\partial C}{\partial x} + \frac{1}{Pe_L}\frac{\partial^2 C}{\partial x^2} + \frac{\eta}{Pe_R}\left(\frac{\partial^2 C}{\partial r^2} + \frac{1}{r}\frac{\partial C}{\partial r}\right) \tag{3}$$

where $C = (C^* - C_{init})/(C_0 - C_{init})$ is the relative concentration. $t = t^*v/L$, $L$ being the length of the column. $x = x^*/L$ is a dimensionless longitudinal coordinate and $r = r^*/R$ is the relative radial position. $Pe_L$ and $Pe_R$ are column Peclet numbers defined as $Pe_L = vL/D_L$ and $Pe_R = vR/D_T$. The ratio of column length to column radius is $\eta = L/R$. Similarly, boundary conditions can be written as

$$C(0, r, t) = H(t) \times \begin{cases} 1 & \text{if } 0 \leqslant r < f \\ 1/2 & \text{if } r = f \\ 0 & \text{if } f < r \leqslant 1 \end{cases} \tag{4a}$$

$$\left.\frac{\partial C(x, r, t)}{\partial r}\right|_{r=1} = 0 \tag{4b}$$

$$\lim_{x\to\infty} C(x, r, t) = 0 \tag{4c}$$

where $f = R_1/R$ is the relative radius of the central inlet zone.

The solution of Eq. (3) subject to Eqs. (4a), (4b), and (4c) for a zero initial relative concentration was recently proposed by Massabo et al. (2006) and requires Bessel series expansion of the inlet radial concentration profile

$$C(0,r,t) = H(t) \times \left( A_0 + \sum_{k=1}^{\infty} A_K J_0\left(Z_1^k r\right) \right) \tag{5}$$

where $J_0$ is the zero-order Bessel function of the first kind and $Z_1^k$ is the $k$th positive root of the first-order Bessel function of the first kind. The Bessel's coefficients for (5) are

$$A_0 = f^2$$
$$A_k = \frac{2fJ_1(fZ_1^k)}{(J_0(Z_1^k))^2 Z_1^k} \tag{6}$$

where $J_1$ is the first-order Bessel function of the first kind. As stressed by Massabo et al. (2006), special attention must be paid to the truncation of this infinite series, as using too few terms would lead to oscillations, resulting in non-physical negative injection concentrations. We use 1000 terms in the series. The relative effluent concentration is defined here as $C_e(r,t) = C(x = 1, r, t)$. Its analytical solution can be expressed as (Massabo et al., 2006)

$$C_e(r,t) = \sum_{k=0}^{\infty} \frac{1}{2} A_k J_0(Z_1^k r) K_k(t) \tag{7}$$

where

$$K_k(t) = \exp\left(\frac{Pe_L}{2}\right) \times \left\{ \begin{array}{l} \exp\left[\sqrt{\frac{Pe_L^2}{4} + \eta (Z_1^k)^2 \frac{Pe_L}{Pe_T}}\right] \\ \times \mathrm{erfc}\left[\frac{1}{2}\sqrt{\frac{Pe_L}{t}} + \sqrt{\frac{Pe_L t}{4} + \frac{\eta}{Pe_T}(Z_1^k)^2 t}\right] \\ + \exp\left[-\sqrt{\frac{Pe_L^2}{4} + \eta (Z_1^k)^2 \frac{Pe_L}{Pe_T}}\right] \\ \times \mathrm{erfc}\left[\frac{1}{2}\sqrt{\frac{Pe_L}{t}} - \sqrt{\frac{Pe_L t}{4} + \frac{\eta}{Pe_T}(Z_1^k)^2 t}\right] \end{array} \right\} \tag{8}$$

Catania et al. (2006) and Massabo et al. (2007) have already tested the use of analytical solutions similar to (7) to determine transport and kinetic parameters from column experiments. They used Monte Carlo techniques to show that local concentration measurements could be confidently used to estimate, among others, longitudinal and transverse dispersivity. However, we need to adapt the solution to surface-averaged effluent concentration measurements.

The average concentration that is measured in an annular zone of the column outlet can be computed according to

$$\begin{aligned} C_{em}(t)|_{r_i,r_o} &= \frac{2}{(r_o^2 - r_i^2)} \int_{r_i}^{r_o} C_e(r,t) r \, dr \\ &= \sum_{k=0}^{\infty} A_k K_k^*(t) \end{aligned} \tag{9}$$

where $r_i$ and $r_o$ are respectively the inner and the outer relative radii of the annular zone of interest and where $K_k^*(t) = K_k(t) \times B_k^{r_i,r_o}$, with

$$B_k^{r_i,r_o} = \left\{ \begin{array}{ll} 1/2 & \text{if } k = 0 \\ \frac{r_o J_1(Z_1^k r_o) - r_i J_1(Z_1^k r_i)}{Z_1^k (r_o^2 - r_i^2)} & \text{if } k \neq 0 \end{array} \right. \tag{10}$$

Eq. (9) in combination with Eqs. (8) and (10) can be fitted to transient effluent concentration data to simultaneously estimate $v$, $\alpha_L$ and $\alpha_T$. Provided $r_i$ and $r_o$ are properly chosen, the solution can be used for any zone division of the outlet flask. In particular, setting $r_i = 0$ and $r_o = 1$ in (9) and (10) leads to an expression for the average concentration over the full column outlet cross-section as a result of an injection over inner zone of the inlet cross-section

$$\begin{aligned} C_{em}(t)|_{0,1} = \frac{f^2}{2} \Bigg[ & \mathrm{erfc}\left(\sqrt{\frac{Pe_L}{4t}} - \sqrt{\frac{Pe_L t}{4}}\right) \\ & + \exp(Pe_L)\mathrm{erfc}\left(\sqrt{\frac{Pe_L}{4t}} + \sqrt{\frac{Pe_L t}{4}}\right) \Bigg] \end{aligned} \tag{11}$$

which is the solution of the advection–dispersion equation corresponding to a one-dimensional continuous injection at a constant relative concentration $f^2$ (Kreft and Zuber, 1978). Eq. (11) shows that the average breakthrough curve computed from the data measured in each annular zone can be analyzed using classical one-dimensional methods to obtain $v$ and $\alpha_L$, independently from the value of the transverse dispersivity.

## Effect of column length and boundary conditions

There are two potential issues when using Eqs. (9) and (11) to analyze concentration data obtained from the setup described in this study: the analytical solutions assume (i) a semi-infinite column, and (ii) a constant injection concentration. The goal of this section is to evaluate the influence of these limitations of the analytical solutions using a numerical model that allows us to depart from the boundary conditions (4a) and (4c). To quantify the bias on estimated values of seepage velocity, longitudinal dispersivity, and transverse dispersivity, we numerically simulate the annulus-and-core test using MODFLOW 2000 (Harbaugh et al., 2000) and MT3DMS (Zheng and Wang, 1999) for columns of finite length and using various boundary conditions. We analyze the synthetic breakthrough curves with the analytical solutions (9) and (11), and compare the estimated transport parameters with the true values used as input of the numerical codes. The column is discretized into $2 \times 2 \times 2$ mm$^3$ cubic cells. The cross-section of the column is discretized in $50 \times 50$ cells. Since it is expected that the bias on estimated transport parameters depends on the length of the column, we varied column length from 10 to 200 cells (2–40 cm), yielding a ratio of column length to diameter $L/D$ ranging from 0.2 to 4. The actual column used in this study is characterized by a ratio $L/D \approx 1$. We used a constant saturated hydraulic conductivity of $10^{-4}$ m/s, an effective porosity of 40% and a gradient of 0.2, similar to the experimental conditions adopted when testing the Brusselean sand. We adopted $\alpha_T = 0.2$ cm and we tested $\alpha_L = 1$, 0.5 and 0.2 cm. Although these values do not cover the whole range of possible values, we believe that, within the scope of this analysis, these variations are sufficient. We kept the effective molecular diffusion coefficient equal to zero. Although numerical issues are not to be expected for grid Peclet numbers between 0.2 and 1, we used the third-order TVD advection scheme of MT3DMS, with a maximum Courant number of 1. The errors $\varepsilon$ on estimated parameters are computed as

$$\varepsilon = \frac{p_{meas} - p_{th}}{p_{th}} \tag{12}$$

where $p$ are the transport parameters ($v$, $\alpha_L$ or $\alpha_T$), and subscripts meas and th refer to measured and theoretical values, respectively. In this case, theoretical values are a priori values used as an input of the numerical model, while measured values are obtained by fitting the analytical solutions (9) and (11) on the numerically simulated breakthrough curves. A positive error indicates that the effect of simplified boundary conditions yields an overestimation of transport parameter values, while a negative error indicates that the estimated value is smaller than the actual value.

First, in order to assess the error associated with the finite length of the column only (boundary condition described by Eq. (4c)), we simulated transport through finite-length columns assuming a constant concentration in the inlet injection zone, similar to Eq. (4a). In order to balance mass through the inlet boundary, this formulation implies that calculated concentrations $C$ are flux-averaged concentrations (Kreft and Zuber, 1978; van Genuchten and Parker, 1984). At the column outlet, we invoke continuity of flux-averaged concentration through the boundary, which also translates into a first-type or Dirichlet condition (Golz and Dorroh, 2001)

$$C_e(r,t) = C(1,r,t) \tag{13}$$

where $C_e$ and $C$ are defined in previous section. For the numerical simulations, this condition implies that effluent concentrations in a given zone are computed as the arithmetic average of concentration in grid cells belonging to that zone. The results are reported in Fig. 3a. It appears that for the ratio $L/D \approx 1$ (corresponding to longitudinal column Peclet numbers of 10, 20, and 50, depending on the longitudinal dispersivity of the material tested) adopted for the experimental setup, the errors associated to the finite length of the column are typically of the order of 10–15%, and increase with longitudinal dispersivity. The proper convergence of estimation errors to zero also show that numerical errors can be considered negligible. We also ran simulations with smaller transverse dispersivity values and observed a slight reduction in estimations errors.

Novakowski (1992a,b) report that analytical solutions corresponding to Dirichlet inlet and outlet conditions are physically not consistent and usually poorly fit experimental data. He indicates that third-type conditions have to be used instead, because these solutions verify mass balance across inlet and outlet boundaries. At the inlet boundary of the numerical model, instead of Eq. (4a), we have for the second set of numerical simulations

$$\left[C(x,r,t) - \frac{1}{Pe_L}\frac{\partial C(x,r,t)}{\partial x}\right]_{x=0} = H(t) \times \begin{cases} 1 & \text{if } 0 \le r < f \\ 1/2 & \text{if } r = f \\ 0 & \text{if } f < r \le 1 \end{cases} \tag{14}$$

where it is now implied that calculated concentrations $C$ are volume-averaged or resident concentrations. At the outlet boundary, we use (Cornaton et al., 2004; Golz and Dorroh, 2001; Novakowski, 1992a,b)

$$C_e(r,t) = \left[C(x,r,t) - \frac{1}{Pe_L}\frac{\partial C(x,r,t)}{\partial x}\right]_{x=1} \tag{15}$$

Practically, concentration gradients in (15) were approximated using a finite-difference method. It appears that the errors associated to the finite length of the column and to the boundary conditions tend to compensate each other (Fig. 3b). For a ratio $L/D = 1$, we now have an error on seepage velocity of about −1% and an error on transverse dispersivity of −1.5%. The error on longitudinal dispersivity is less affected by the injection boundary condition and remains

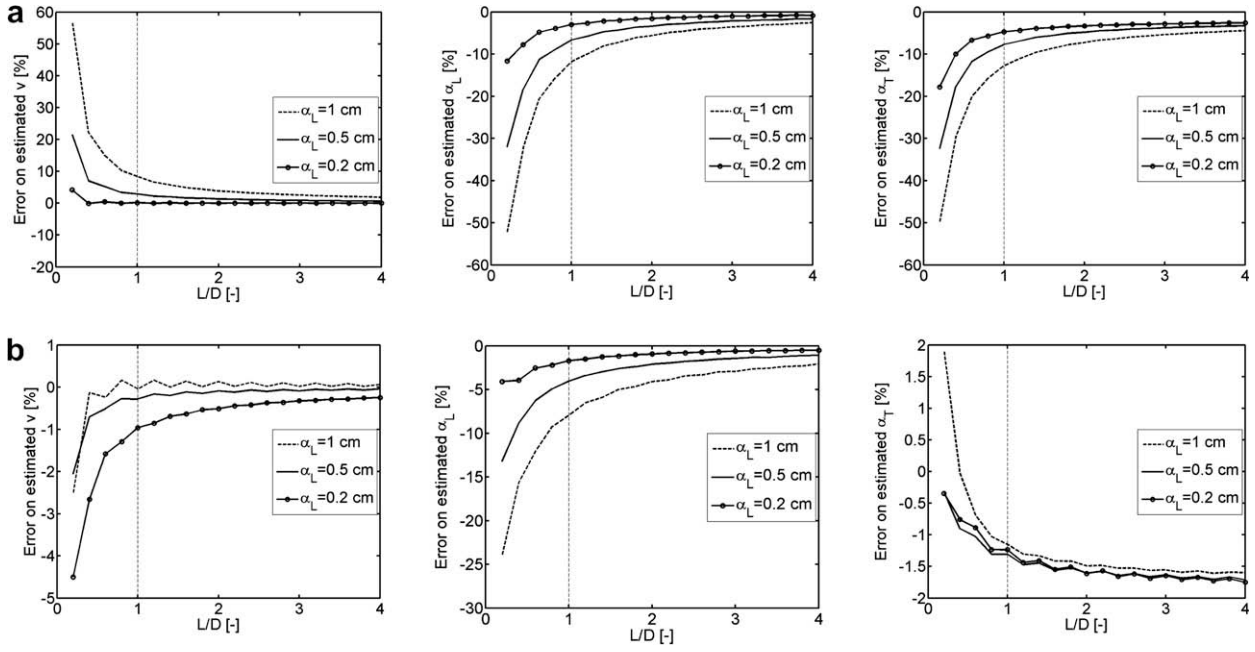


**Figure 3** Errors on estimated transport parameters. (a) Errors resulting from the finite length of the column. (b) Errors resulting from the finite length of the column and from the Dirichlet inlet and outlet boundary conditions.

between −2% and −10%. The negative signs also indicate that estimated values are smaller than actual values. For the case of seepage velocity, this also implies that effective porosities are slightly overestimated.

As a summary, it appears that, for the column geometry adopted in this study, estimation errors resulting from the use of the analytical solutions (9) and (11) are expected to be below other experimental errors and below errors linked e.g. to sample heterogeneity. However, the sensitivity analysis performed on the column length $L$ revealed that columns with a ratio $L/D$ smaller than 1 should not be used.

## General methodology for the analysis of effluent data

Bulk concentration measurements have to be corrected in order to account for perturbations induced by the experimental device itself. We use the total flux $Q$ through the sample to shift the breakthrough curves by the purge time of the dead volumes (outlet zones and tubing) according to

$$C_{em}(t^*)|_{\text{zone } i} = C_{\text{meas}}(t^* + \tau_i)|_{\text{zone } i} \tag{16}$$

where $C_{\text{meas}}$ is the concentration measured by the sensor and $\tau_i = 3V_i/Q$. $V_i$ is the volume of the $i$th outlet zone, which includes the volume of the tubing between the flask and the sensor. For the sake of clarity, we have used $t^*$ instead of the dimensionless time $t$ in (16). The total flux $Q$ is also used to compute actual injection conditions in the central zone according to (Novakowski, 1992a,b)

$$C_0(0, r, t^*) = C_0\left(1 - \exp\left(-\frac{t^*}{\tau_{\text{in}}}\right)\right) \quad \text{if } 0 \le r < f \tag{17}$$

where $\tau_{\text{in}} = 3V_{\text{in}}/Q$, $V_{\text{in}}$ being the volume of the inlet injection zone. Since the advection–dispersion equation is linear in concentration $C$, the corresponding solution to the transport equation is obtained using a principle of superposition: the exponential injection condition (17) is discretized into a sum of small injection steps, and outlet breakthrough curves are computed by summing the individual solutions (Eq. (9) or Eq. (11), depending on the dimensionality of the test) corresponding to each small injection step. This procedure is equivalent to convolving the transport solution corresponding to a Dirac injection condition with (17). This semi-analytical procedure was coded as a MATLAB function.

As a summary, we propose here a three-step methodology for the analysis of experimental data collected from the annulus-and-core device:

1. The mean experimental breakthrough curve is computed by averaging the data recorded in each outlet zone (preliminary shifted according to the total discharge). This curve is analyzed to determine seepage velocity $v$ and longitudinal dispersivity $\alpha_L$, using the semi-analytical solution corresponding to (11) and (17). This procedure is achieved by least-square fitting of the solution to the data, using the built-in MATLAB nonlinear optimization function *lsqcurvefit*. This function uses a Gauss–Newton algorithm. It must be noted that the length of the penetrating skirts was removed from the column length to perform the calculation.
2. The semi-analytical solutions corresponding to (9) and (17) for each outlet zone are simultaneously fitted on the three outlet curves (shifted according to the total discharge), using the values of $v$ and $\alpha_L$ previously determined, to obtain the estimated transverse dispersivity $\alpha_T$. This procedure is achieved using the same MATLAB optimization function. Again the column length accounted for in the calculation was decreased according to the length of the penetrating skirts.
3. Finally, the effective porosity $n_e$ is obtained by dividing Darcy velocity $Q/A$ by the seepage velocity $v$ obtained in step 1. This requires the retardation factor to be equal to 1, which can be reasonably assumed considering the low reactivity of the tracer adopted and the granular media tested. The total flux $Q$ is also used to compute the hydraulic conductivity $K$ of the sample when a gradient measurement $i$ is available.

## Preliminary experiments and discussion

Table 2 summarizes the experimental conditions and the results of the tests performed. In a first stage, one-dimensional transport experiments are carried out using a single injection flask, instead of the divided one presented above. Individual breakthrough curves recorded in each outlet zone are analyzed independently, leading to a total of three sets of parameters ($v$, $\alpha_L$) for each concentration step. We did not observe systematic trends in seepage velocity. Concentration values collected in the outer annulus are not systematically larger than in inner zones, which shows the usefulness of the silicone grease used to prevent preferential flow along the rigid column walls. However, longitudinal dispersivity values computed from data collected in the outer annulus are always larger than the values obtained from concentration in the center core zone and in the intermediate annulus, probably because of a larger mixing time in the outer annulus resulting from a larger volume of that zone. Therefore, average seepage velocities and longitudinal dispersivities reported in Table 2 for one-dimensional tests are computed from center and intermediate zone data only.

Fig. 4 shows a set of typical experimental data recorded during a two-dimensional test. Steady-state average concentration levels are usually found to differ from $f^2$ within less than 3%, attesting mass conservation. It appears that the fitting procedure used to estimate $\alpha_T$ usually leads to an underestimation of the steady-state concentration level in the intermediate zone and a slight overestimation of concentration in the outer annulus. It also appears that, if the transient part of the average curve is properly fitted, the longitudinal spreading of individual curves (i.e. the transient part of the curves) is usually underestimated. This observation will be further discussed below.

Total porosities $n$ were computed by weighing the column system, knowing the specific weight of the granular material tested and the internal volume of the column. Effective porosities $n_e$ computed from the measured seepage velocities are very close to total porosities, indicating that samples are correctly saturated. Although $n_e > n$ could indicate that the retardation factor is actually slightly larger than 1, the results of the numerical simulations showed that effective porosities can be overestimated, as a result of the

**Table 2** Experimental conditions and results of one- and two-dimensional tests

| Sample | | Concentration | | Flow | | | Porosity | | Dispersivity | |
|---|---|---|---|---|---|---|---|---|---|---|
| | | $C_{init}$ (g/l) | $C_0$ (g/l) | $Q$ (cm$^3$/s) | $i$ (—) | $K$ (mm/s) | $n$ (%) | $n_e$ (%) | $\alpha_L$ (mm) | $\alpha_T$ (mm) |
| GB1A | 1D | 0.60 | 0.73 | 1.64 | <0.02 | — | 40.6 | 42.1 | 15.9 | — |
| GB1B | 1D | 0.73 | 0.94 | 1.64 | <0.02 | — | 40.6 | 42.2 | 17.6 | — |
| GB2A | 1D | 0.49 | 0.56 | 1.65 | <0.02 | — | 39.7 | 40.7 | 24.8 | — |
| GB2B | 1D | 0.62 | 0.75 | 1.65 | <0.02 | — | 39.7 | 40.7 | 21.6 | — |
| GB3A | 1D | 0.49 | 0.57 | 1.67 | <0.02 | — | 37.5 | 38.0 | 19.9 | — |
| GB3B | 1D | 0.63 | 0.85 | 1.67 | <0.02 | — | 37.5 | 38.0 | 18.8 | — |
| GB4A | 2D | 0.63 | 0.77 | 1.33 | <0.02 | — | 36.2 | 39.0 | 30.4 | 3.63 |
| GB4B | 2D | 0.77 | 0.89 | 1.28 | <0.02 | — | 36.2 | 37.8 | 31.1 | 5.11 |
| GB5A | 2D | 0.47 | 0.58 | 1.24 | <0.02 | — | 34.2 | 35.9 | 25.5 | 1.76 |
| GB5B | 2D | 0.68 | 0.78 | 1.25 | <0.02 | — | 34.2 | 37.8 | 60.4 | 2.70 |
| GB6A | 2D | 0.45 | 0.60 | 1.25 | <0.02 | — | 35.3 | 30.7 | 14.5 | 2.03 |
| GB6B | 2D | 0.71 | 0.84 | 1.24 | <0.02 | — | 35.3 | 39.0 | 25.1 | 3.16 |
| GS1A | 1D | 0.49 | 0.58 | 1.58 | <0.02 | — | 40.2 | 40.9 | 9.77 | — |
| GS1B | 1D | 0.68 | 0.80 | 1.61 | <0.02 | — | 40.2 | 41.0 | 8.00 | — |
| GS2A | 1D | 0.52 | 0.56 | 1.60 | <0.02 | — | 40.5 | 39.9 | 9.51 | — |
| GS2B | 1D | 0.62 | 0.84 | 1.60 | <0.02 | — | 40.5 | 41.4 | 7.88 | — |
| GS3A | 2D | 0.57 | 0.61 | 1.25 | <0.02 | — | 40.4 | 45.0 | 27.3 | 2.09 |
| GS3B | 2D | 0.61 | 0.77 | 1.25 | <0.02 | — | 40.4 | 43.3 | 34.9 | 2.12 |
| GS4A | 2D | 0.57 | 0.63 | 1.26 | <0.02 | — | 39.5 | 35.3 | 18.0 | 1.60 |
| GS4B | 2D | 0.63 | 0.74 | 1.24 | <0.02 | — | 39.5 | 43.6 | 16.8 | 1.43 |
| GS5A | 2D | 0.58 | 0.72 | 1.26 | <0.02 | — | 39.2 | 38.3 | 17.7 | 2.48 |
| GS5B | 2D | 0.72 | 0.93 | 1.24 | <0.02 | — | 39.2 | 36.1 | 14.5 | 3.59 |
| BS1A | 1D | 0.62 | 0.72 | 0.53 | 0.28 | 0.232 | 36.0 | 34.9 | 3.66 | — |
| BS1B | 1D | 0.72 | 0.79 | 0.54 | 0.34 | 0.197 | 36.0 | 31.2 | 2.45 | — |
| BS2A | 1D | 0.52 | 0.59 | 0.53 | 0.23 | 0.284 | 36.1 | 30.6 | 2.54 | — |
| BS2B | 1D | 0.65 | 0.72 | 0.55 | 0.33 | 0.206 | 36.1 | 33.6 | 2.45 | — |
| BS3A | 1D | 0.44 | 0.54 | 0.58 | 0.16 | 0.449 | 36.1 | 33.7 | 3.25 | — |
| BS3B | 1D | 0.54 | 0.82 | 0.57 | 0.19 | 0.361 | 36.1 | 32.2 | 2.43 | — |
| BS3C | 1D | 0.82 | 0.92 | 0.56 | 0.21 | 0.334 | 36.1 | 36.3 | 4.09 | — |
| BS4A | 1D | 0.62 | 0.78 | 0.57 | 0.18 | 0.390 | 36.1 | 33.7 | 3.88 | — |
| BS4B | 1D | 0.78 | 0.83 | 0.55 | 0.19 | 0.361 | 36.1 | 30.8 | 4.52 | — |
| BS4C | 1D | 0.83 | 0.87 | 0.57 | 0.22 | 0.325 | 36.1 | 35.3 | 6.44 | — |
| BS5A | 2D | 0.54 | 0.72 | 1.00 | 0.33 | 0.379 | 37.0 | 33.8 | 6.98 | 0.75 |
| BS5B | 2D | 0.72 | 0.77 | 1.01 | 0.34 | 0.365 | 37.0 | 39.0 | 5.00 | 1.10 |
| BS6A | 2D | 0.54 | 0.72 | 0.98 | 0.40 | 0.299 | 37.1 | 33.8 | 4.26 | 0.95 |
| BS6B | 2D | 0.72 | 0.84 | 1.01 | 0.46 | 0.273 | 37.1 | 37.2 | 1.31 | 0.87 |
| BS7A | 2D | 0.59 | 0.66 | 1.03 | 0.53 | 0.241 | 37.0 | 34.9 | 4.17 | 1.07 |
| BS7B | 2D | 0.66 | 0.83 | 1.03 | 0.53 | 0.241 | 37.0 | 41.2 | 3.02 | 1.11 |
| BS7C | 2D | 0.83 | 0.91 | 1.03 | 0.53 | 0.241 | 37.0 | 39.8 | 4.21 | 1.27 |

GB stands for glass beads, GS for gravel sand and BS for Brusselean sand. Letters A, B, and C refer to separate tests performed on the same sample. Hydraulic conductivity of GB and GS could not be accurately computed, due to the very low gradient resulting from the flow rate used for the tests.

boundary conditions of the analytical solution used. We also usually have $n_e < n$ for Brusselean sand samples, which tends to indicate a lower saturation. Air bubbles are more difficult to extract from Brusselean sand samples due to smaller pore sizes.

The examination of the results reported in Table 2 shows that the usual correlation between longitudinal dispersivity and particle size distribution is observed: the material with the smallest mean grain diameter $d_{50}$ is characterized by a smaller longitudinal dispersivity (Perkins and Johnston, 1963; Xu and Eckstein, 1997). The longitudinal dispersivities for the Brusselean sand are in the typical range reported by Bromly et al. (2007) for this type of experimental device. However, for the glass beads, we obtain $\alpha_L$ values larger than those reported by Xu and Eckstein (1997) for a similar porous medium, measured using a 310 mm-long column of 63 mm diameter. Based on a compilation of 291 laboratory column experiments, Bromly et al. (2007) showed that such a discrepancy could originate from the experimental device itself. Bromly et al. (2007) observed a significant scale effect in longitudinal dispersivity with column diameter. They also observed that columns of a length less than approximately 10 cm generally result in greater dispersivities than longer columns. Bromly et al. (2007) attributed this effect to the analytical solution used to estimate $\alpha_L$, which assumes an infinite column length. However, the results of

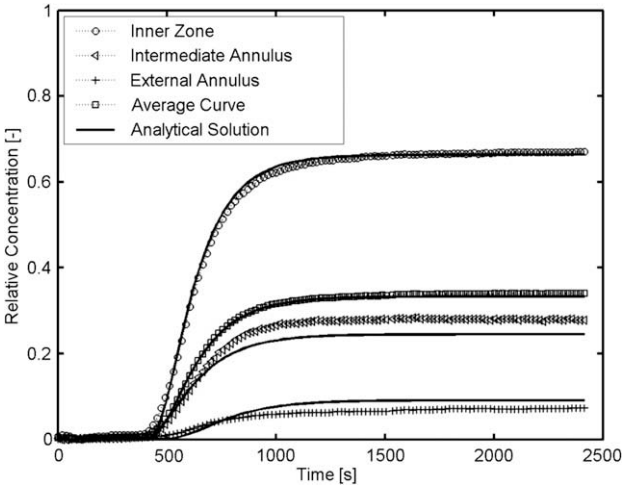


**Figure 4** Typical breakthrough recorded during a 2D test: sample BS5A.

the numerical simulations performed in this study showed that longitudinal dispersivity values obtained using such analytical solutions should be underestimated. We suspect that an improper incorporation of mixing conditions like (17) might be the actual reason for higher dispersivity values (Novakowski, 1992a,b). For the setup presented in this paper, it is expected that the presence of the penetrating skirts also induce some variability on the velocity field, eventually resulting in larger estimated $\alpha_L$ values.

The packing of non-spherical particles usually lead to greater dispersion than do packs of spherical particles of about the same size (Perkins and Johnston, 1963; Xu and Eckstein, 1997). We therefore expect the dispersivity of the gravel sand to be larger than that of the glass beads. We observe the opposite trend: the dispersivity of the gravel sand is about twice as small as that of the glass beads. The outlet annular zones have relatively close radii: the intermediate zone has a width of 12.1 mm, whereas the outer zone has a width of 9.3 mm. Since the gravel sand contains particles of a size larger than 3 mm, we suspect that local wall effects on the penetrating skirts might locally increase porosity and therefore induce a bias on the shape of concentration distributions.

It is also appears from the results in Table 2 that longitudinal dispersivities from 2D tests are usually larger than the values obtained from 1D tests. In one-dimensional tests, $\alpha_L$ is computed from individual breakthrough curves, whereas it is computed from an averaged curve in 2D tests. Bulk experimental data are shifted according to the total flux across the sample and the respective sizes of the dead volumes. An error on the measurement of $Q$, an error on the measurement of the dead volumes, or the presence of local heterogeneities, which can yield a higher local discharge in one of the outlet zone, results in an error in the temporal shift of the breakthrough curve. Averaging out breakthrough curves that do not have the same mean breakthrough time typically results in a larger apparent longitudinal dispersivity. Indeed, we noticed in Fig. 4 that, although the average concentration curve is correctly matched, there are some discrepancies in the transient segment of individual curves.

Although we still observe from the data summarized in Table 2 a correlation between $\alpha_T$ and particle size, the values span a smaller range: the longitudinal dispersivity of the glass beads is more than 5—6 times larger than that of the Brusselean sand, whereas the transverse dispersivity of the glass beads is only 2—3 times larger than that of the

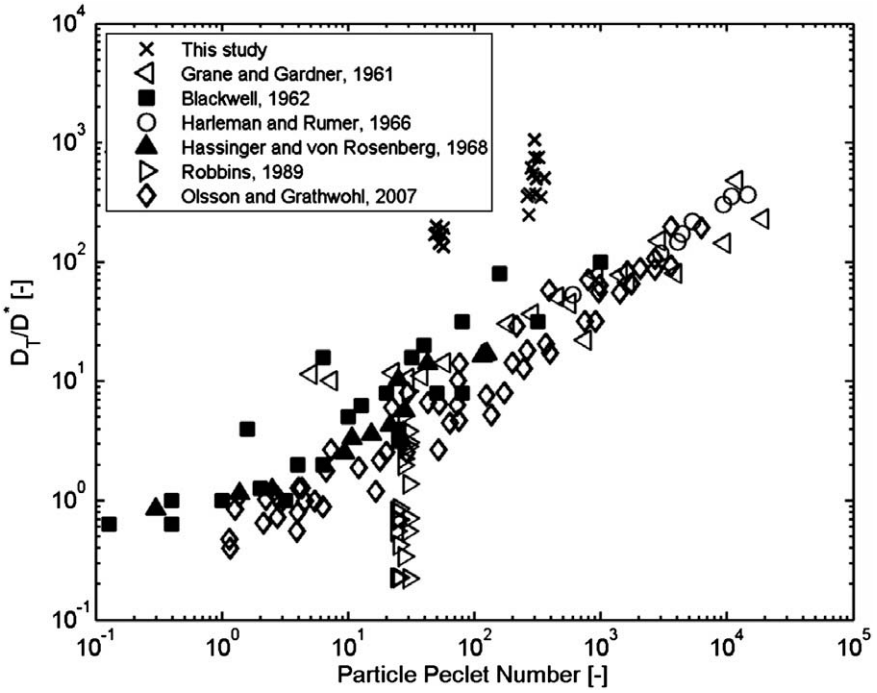


**Figure 5** Transverse dispersion coefficients obtained from two-dimensional tests, compared to results previously reported in the literature.

Brusselean sand. We obtain ratios of longitudinal to transverse dispersivity ranging between 6.08 and 22.37 for the glass beads, 4.04 and 16.46 for the gravel sand, and 1.51 and 9.31 for the Brusselean sand. Most of these figures fall within the general rule-of-thumb interval of 6–20 (Fetter, 1999).

We compute particle Peclet numbers according to

$$Pe_P = \frac{v d_{50}}{D^*} \quad (18)$$

and adopt $D^* = 2.03 \times 10^{-9}$ m$^2$/s as the coefficient of molecular diffusion of chloride in free water at 25 °C (Xu and Eckstein, 1997). We obtain larger transverse dispersion coefficients than previously reported in the literature (Fig. 5). Even for a regular material such as glass beads, and even if the material is carefully packed, we cannot deny that heterogeneities are present. Slight fluctuations of hydraulic conductivity cause plume meandering and progressive distortion of transverse concentration profiles. The mean travel path of the plume deviates from the axis of the column, which results in a lower and a larger concentration level in the inner and the intermediate outlet annuli respectively, as we observed in Fig. 4. Transverse advective shifts of the plumes are then assimilated to larger apparent transverse dispersivity values. This assumption is consistent with the observation that other annulus-and-core methods (shown using black markers in Fig. 5) also yield transverse dispersion coefficients larger than the average.

Most methods for the determination of transverse dispersivity yield smaller $\alpha_T$ estimates because they involve concentration measurements within the soil sample. For example, Robbins' method (1989) is based on local (point) measurements inside the column body, along the theoretical centerline of the mean plume path. If the actual center of the plume is slightly off this theoretical line, the error is relatively small. Indeed, the shape of the transverse concentration distribution is relatively smooth close to the peak (at the peak, spatial concentration gradients are equal to zero). A concentration measurement at a location close to the peak is likely to be very similar to the peak value and the effect of plume meandering is expected to be small. Moreover, when a sufficiently detailed transverse concentration profile can be obtained within the column, data can be corrected to account for peak offset (Harleman and Rumer, 1963; Olsson and Grathwohl, 2007). When using annulus-and-core devices, a small transverse dispersivity yields a small concentration in the annulus. But a slight movement of the plume off its centerline might result in a dramatic increase of the concentration in the annulus. While most of the laboratory methods allow the determination of what is commonly referred to an ''effective dispersion coefficient'' in the stochastic hydrology literature, annulus-and-core devices provide estimates of ''macrodispersion coefficient''. The latter includes measures of both transverse dispersion and uncertainty in the mean transverse position of the plume. It is moreover suspected that having divided the outlet flask in three zones rather than two further enhance the effect of plume meandering on estimated $\alpha_T$ values. Indeed, looking at a typical result such as the one shown in Fig. 4, fitting the analytical solution on data recorded in the inner and intermediate zones only, should yield smaller apparent transverse dispersivities.

## Conclusions

In this paper, we describe a column method to simultaneously determine longitudinal and transverse dispersivities of porous materials. The experimental device is an extension of the ''annulus-and-core'' method proposed by Blackwell (1962) and Hassinger and von Rosenberg (1968). The inlet and outlet cross-sections of the column are divided into three equal concentric areas. Although the device allows for a wide range of flow and tracer injection conditions, we only tested in this study uniform flow conditions with a continuous tracer injection in the inner inlet zone.

Experimental results are analyzed using an analytical solution based on Massabo et al. (2006) developments. We found that concentration data averaged over the entire outlet could be analyzed using classical one-dimensional methods, which makes the determination of the velocity and of the longitudinal dispersivity independent of the transverse dispersivity. The appropriateness of the solutions was shown with the aid of numerical simulations performed using MODFLOW 2000 and MT3DMS.

We tested the setup using three different materials. We used 1.5-mm-diameter glass beads, a gravel sand and a medium sand. Longitudinal dispersivity values are consistent with previously published data, although it is shown that $\alpha_L$ values determined from 2D tests have a larger uncertainty than those determined from classical one-dimensional column tests. The curve used to estimate longitudinal dispersivity is computed as the average of the curves recorded in each outlet zone. It is expected that potential experimental errors in each curve sum up, resulting in a larger uncertainty for the average curve, and therefore in a larger uncertainty for $\alpha_L$. This larger uncertainty is however balanced by the advantages of the method, namely the rapidity of the test, its potentially low cost, and the ability to simultaneously obtain measurements of all three transport parameters. Transverse dispersivity data are larger than the values reported for other column devices. However, a careful examination of transverse dispersion coefficients obtained using other annulus-and-core devices showed that they are generally larger than the average, supposedly as a result of plume meandering. Future work is currently planned to verify this hypothesis: numerical simulations of laboratory methods for the determination of transverse dispersivity will be performed using synthetic heterogeneous soil samples, to assess the variability of effective transport parameters as a function of the laboratory method used.

## Acknowledgments

Christophe Frippiat was supported by the National Science Foundation of Belgium (Fonds National de la Recherche Scientifique, FRS-FNRS, Belgium, grants no 1.1.216.03.F, 1.1.216.05.F and 1.2.035.07.F). The peristaltic pump was borrowed from Dr. Marnik Vanclooster (UCL, Louvain-la-Neuve, Belgium). The authors wish to thank Eugène Bouchonville and Francis Goffin of the Laboratory of Civil Engineering (UCL, Louvain-la-Neuve, Belgium) and Grégory Gillet and Sébastien Louppe for their participation in the early developments of this device.

## References


ASTM, 2000. D2434-68: Standard test methods for permeability of granular soils (constant head). In: Annual Book of ASTM Standards 04.08, pp. 232–236.

ASTM, 2002. D1557: Standard test methods for laboratory compaction characteristics of soil using modified effort. In: Annual Book of ASTM Standards 04.08, pp. 133–142.

Baumeister, E., Klose, U., Albert, K., Bayer, E., Guiochon, G., 1995. Determination of the apparent transverse and axial dispersion coefficients in a chromatographic column using pulsed field gradient magnetic resonance. Journal of Chromatography 694, 321–331.

Benekos, I.D., Cirpka, O.A., Kitanidis, P.K., 2006. Experimental determination of transverse dispersivity in a helix and a cochlea. Water Resources Research 42, W07406. doi:10.1029/2005/WR00471.

Blackwell, R.J., 1962. Laboratory studies of microscopic dispersion phenomena. Society of Petroleum Engineers Journal 2 (1), 1–8.

Bromly, M., Hinz, C., Aylmore, L.A.G., 2007. Relation of dispersivity to properties of homogeneous saturated repacked soil columns. European Journal of Soil Science 58, 293–301.

Bruch, J.C., 1970. Two-dimensional dispersion experiments in a porous medium. Water Resources Research 6 (3), 791–800.

Catania, F., Massabo, M., Paladino, O., 2006. Estimation of transport and kinetic parameters using analytical solutions of the 2D advection-dispersion-reaction model. Environmetrics 17, 199–216.

Cirpka, O.A., Frind, E.O., Helmig, R., 1999. Numerical simulation of biodegradation controlled by transverse mixing. Journal of Contaminant Hydrology 40, 159–182.

Cirpka, O.A., Kitanidis, P.K., 2001. Theoretical basis for the measurement of local transverse dispersion in isotropic porous media. Water Resources Research 37 (2), 243–252.

Cirpka, O.A., Olsson, A., Ju, Q., Rahman, M.A., Grathwohl, P., 2006. Determination of transverse dispersion coefficients from reactive plume length. Ground Water 44 (2), 212–221.

Cornaton, F., Perrochet, P., Diersch, H.-J., 2004. A finite-element formulation of the outlet gradient boundary condition for convective–diffusive transport problems. International Journal for Numerical Methods in Engineering 61, 2716–2732.

Delgado, J.M.P.Q., Guedes de Carvalho, J.R.F., 2001. Measurement of the coefficient of transverse dispersion in flow through packed beds for a wide range of values of the Schmidt number. Transport in Porous Media 44, 165–180.

de Rooij, G.H., Stagnitti, F., 2002. Spatial and temporal distribution of solute leaching in heterogeneous soils: analysis and application to multisampler lysimeter data. Journal of Contaminant Hydrology 54, 329–346.

Fetter, C.W., 1999. Contaminant Hydrogeology, second ed. Prentice Hall, Upper Saddle River.

Gelhar, L.W., Gutjahr, A.L., Naff, R.L., 1979. Stochastic analysis of macrodispersion in a stratified aquifer. Water Resources Research 15 (6), 1387–1397.

Golz, W.J., Dorroh, J.R., 2001. The convection–diffusion equation for a finite domain with time varying boundaries. Applied Mathematical Letters 14, 983–988.

Grane, F.E., Gardner, G.H.F., 1961. Measurement of transverse dispersion in granular media. Journal of Chemical and Engineering Data 6 (2), 283–287.

Guedes de Carvalho, J.R.F., Delgado, J.M.P.Q., 1999. Mass transfer from a large sphere buried in a packed bed along which liquid flows. Chemical Engineering Science 54, 1121–1129.

Guedes de Carvalho, J.R.F., Delgado, J.M.P.Q., 2000. Lateral dispersion in liquid flow through packed beds at Pem < 1400. AIChE Journal 46 (5), 1089–1095.

Han, N.-W., Bhakta, J., Carbonell, R.G., 1985. Longitudinal and lateral dispersion in packed beds: effect of column length and particle size distribution. AIChE Journal 31 (2), 277–288.

Harbaugh, A.W., Banta, E.R., Hill, M.C., McDonald, M.G., 2000. MODFLOW-2000, the US Geological Survey modular groundwater model: user guide to modularization concepts and the ground-water flow processes. US Geological Survey Open-File Report 00-92.

Harleman, D.R.F., Rumer, R.R., 1963. Longitudinal and lateral dispersion in an isotropic porous medium. Journal of Fluid Mechanics 16, 385–394.

Hassinger, R.C., von Rosenberg, D.U., 1968. A mathematical and experimental investigation of transverse dispersion coefficients. Society of Petroleum Engineers Journal 8 (2), 195–204.

Istok, J.D., Humphrey, M.D., 1995. Laboratory investigation of buoyancy-induced flow (plume sinking) during two-well tracer tests. Ground Water 33 (4), 597–604.

Jiao, J.J., 1993. Data-analyses methods for determining two-dimensional dispersive parameters. Ground Water 31 (1), 57–62.

Kelly, W.E., Mazac, O., Mares, S., 1994. Discussion of ''Estimation of dispersion parameters for two-dimensional plumes'' by S. Zou and A. Parr. Ground Water 32 (2), 328–329.

Kim, S.-B., Jo, K.-H., Kim, D.-J., Jury, W.A., 2004. Determination of two-dimensional laboratory-scale dispersivities. Hydrological Processes 18, 2475–2483.

Klenk, I.D., Grathwohl, P., 2002. Transverse vertical dispersion in groundwater and the capillary fringe. Journal of Contaminant Hydrology 58, 111–128.

Kreft, A., Zuber, A., 1978. On the physical meaning of the dispersion equation and its solutions for different initial and boundary conditions. Chemical Engineering Science 33, 1471–1480.

Massabo, M., Cianci, R., Paladino, O., 2006. Some analytical solutions for two-dimensional convection–dispersion equation in cylindrical geometry. Environmental Modelling and Software 21 (5), 681–688.

Massabo, M., Catania, F., Paladino, O., 2007. A new method for laboratory estimation of the transverse dispersion coefficient. Ground Water 45 (3), 339–347.

McCarthy, K., Johnson, R.L., 1993. Transport of volatile compounds across the capillary fringe. Water Resources Research 29 (6), 1675–1683.

Novakowski, K.S., 1992a. An evaluation of boundary conditions for one-dimensional solute transport. 1. Mathematical developments. Water Resources Research 28 (9), 2399–2410.

Novakowski, K.S., 1992b. An evaluation of boundary conditions for one-dimensional solute transport. 2. Column experiments. Water Resources Research 28 (9), 2411–2423.

Oliviera, I.B., Demond, A.H., Salehzadeh, A., 1996. Packing of sands for the production of homogeneous porous media. Soil Science Society of America Journal 60, 49–53.

Olsson, A., Grathwohl, P., 2007. Transverse dispersion of non-reactive tracers in porous media: a new nonlinear relationship to predict dispersion coefficients. Journal of Contaminant Hydrology 92, 149–161.

Oostrom, M., Dane, J.H., Güven, O., Hayworth, J.S., 1992. Experimental investigation of dense solute plumes in an unconfined aquifer. Water Resources Research 28 (9), 2315–2326.

Oostrom, M., Hofstee, C., Walker, R.C., Dane, J.H., 1999a. Movement and remediation of trichloroethylene in a saturated homogeneous porous medium. 1. Spill behavior and initial dissolution. Journal of Contaminant Hydrology 37, 159–178.

Oostrom, M., Hofstee, C., Walker, R.C., Dane, J.H., 1999b. Movement and remediation of trichloroethylene in a saturated homogeneous porous medium. 2. Pump-and-treat and surfactant flushing. Journal of Contaminant Hydrology 37, 179–197.

Pearce, A.E., Voudrias, E.A., Whelan, M.P., 1994. Dissolution of TCE and TCA pools in saturated subsurface systems. Journal of Environmental Engineering 120 (5), 1191–1206.

Perkins, T.K., Johnston, O.C., 1963. A review of diffusion and dispersion in porous media. Society of Petroleum Engineers Journal 3 (1), 70–84.

Pisani, S., Tosi, N., 1994. Two methods for the laboratory identification of transversal dispersivity. Ground Water 32 (3), 431–438.

Robbins, G.A., 1989. Methods for determining transverse dispersion coefficients of porous media in laboratory column experiments. Water Resources Research 25 (6), 1249–1258.

Schulze-Makuch, D., 2005. Longitudinal dispersivity data and implications for scaling behavior. Ground Water 43 (3), 443–456.

Seagren, E.A., Rittmann, B.E., Valocchi, A.J., 1999. An experimental investigation of NAPL pool dissolution enhancement by flushing. Journal of Contaminant Hydrology 37, 111–137.

van Genuchten, M.T., Parker, J.C., 1984. Boundary conditions for displacement experiments through short laboratory soil columns. Soil Science Society of America Journal 48, 703–708.

Xu, M., Eckstein, Y., 1997. Statistical analysis of the relationships between dispersivity and other physical properties of porous media. Hydrogeology Journal 5 (4), 4–20.

Zhang, X., Qi, X., Zhou, X., Pang, H., 2006. An in situ method to measure the longitudinal and transverse dispersion coefficients of solute transport in soil. Journal of Hydrology 328, 614–619.

Zheng, C., Wang, P.P., 1999. MT3DMS – a modular three dimensional multispecies transport model for simulation of advection, dispersion and chemical reactions of contaminants in ground-water systems: documentation and user's guide. Jacksonville, Florida, US Army Corps of Engineers Contract Report SERDP–99–1.

Zou, S., Parr, A., 1993. Estimation of dispersion parameters for two-dimensional plumes. Ground Water 31 (3), 389–392.

Zou, S., Parr, A., 1994. Two-dimensional dispersivity estimation using tracer experiment data. Ground Water 32 (3), 367–373.